Dynamic solar Primakoff process

Zheng-Liang Liang[1,*] and Lin Zhang[2,3,†]

[1]*College of Mathematics and Physics, Beijing University of Chemical Technology, Beijing 100029, China*
[2]*School of Science, Shenzhen Campus of Sun Yat-sen University, Shenzhen 518107, China*
[3]*Sun Yat-sen University, Guangzhou 510275, China*

(Received 5 January 2024; accepted 4 March 2024; published 4 April 2024)

The Primakoff mechanism is one of the primary channels for the production of solar axions. In canonical estimations of the Primakoff photon-axion conversion rate, the recoil effect is neglected and a static structure factor in adopted. By use of linear response theory, we provide a dynamic description of the solar Primakoff process. It is found that the collective electrons overtake ions as the dominant factor, in contrast to the static screening picture, where ions contribute more to the photon-axion conversion. Nonetheless, the resulting axion flux is only 1% to 2% lower than the standard estimate based on the static structure factor.

DOI: 10.1103/PhysRevD.109.083005

I. INTRODUCTION

The QCD axion that emerged originally as a solution to the strong-CP problem [1–3] is also well promoted as a promising dark matter candidate [4–7] alternative to weakly interacting massive particles, and has attracted increased interest on both theoretical and experimental fronts in recent years. The rich phenomenology of axion can leave peculiar traces in cosmology, astroparticle physics, and particle physics [8–14].

The Sun is the primary natural source for terrestrial axion detection. With a coupling to standard model particles, axions can be produced in the solar interior through a number of channels, such as the Primakoff process [15,16] and the axiorecombination, bremsstrahlung, and Compton scattering process [17,18]. For Kim-Shifman-Vainshtein-Zakharov axions [19,20], the former reaction dominates, while for the Dine-Fischler-Srednicki-Zhinitsky axions [21,22], the latter mechanism dominates. In this paper, we focus on the Primakoff axion production mechanism, where photons convert to axions through the Coulomb field sourced by the charged particles (i.e., electrons and ions).

In conventional wisdom [8,10], the charged particles in the Sun are so heavy compared to the energies of ambient photons that they can be regarded as fixed, in which case the photon energy in a scattering event is considered equal to that of the emitted axion, and the differential cross section of the Primakoff process $\mathrm{d}\sigma_{\gamma\to a}(\mathbf{p}_\gamma)/\mathrm{d}\Omega$ is proportional to $|\mathbf{p}_\gamma \times \mathbf{p}_a|^2/Q^4$, with $\mathbf{p}_\gamma$ and $\mathbf{p}_a$ being the momenta of the incident photon and emitted axion, respectively, and $Q = |\mathbf{Q}| = |\mathbf{p}_\gamma - \mathbf{p}_a|$. In the massless limit of an axion, the cross section is divergent due to the long-range Coulomb interaction. This Coulomb potential can be regulated if the solar in-medium screening effect is taken into account. Raffelt [8] argued that the implication of the screening effect on the differential cross section is described by the following substitution:

$$\frac{|\mathbf{p}_\gamma \times \mathbf{p}_a|^2}{Q^4} \to \frac{|\mathbf{p}_\gamma \times \mathbf{p}_a|^2}{Q^4} S(\mathbf{Q}) = \frac{|\mathbf{p}_\gamma \times \mathbf{p}_a|^2}{Q^4} \frac{1}{1+\kappa^2/Q^2}, \tag{1}$$

where the Debye-Hückel scale κ can be as large as $\sim$9 keV at the solar center and effectively provides a cutoff of the Coulomb interaction. Note that this description is based on the assumption of a negligible recoil effect in the solar medium, and thus a static structure factor $S(\mathbf{Q}) = (1+\kappa^2/Q^2)^{-1}$ is introduced to measure the correlation between the charged particle density [10].

In Ref. [23], Raffelt further considered finite energy shifts in the axion production process in the presence of classical electric-field fluctuations in the solar plasma, so the collective electron motion and the its implication for the axion conversion are unified under a general framework. Moreover, by use of the Kramers-Kronig relations that relate the spectral densities in the electromagnetic

*liangzl@mail.buct.edu.cn
†zhanglin57@mail.sysu.edu.cn

fluctuation description to the static structure factor $S(\mathbf{Q})$, Raffelt reasoned that the Primakoff production rate in Ref. [8] agrees with the total rates of the decay process $\gamma_t(\text{transverse plasmon}) \to \gamma_l(\text{longitudinal plasmon}) + a(\text{axion})$, the plasma coalescence process $\gamma_t + \gamma_l \to a$, and the individual Primakoff process $\gamma_t + e/N(\text{electron/ion}) \to a + e/N$. Thus, as far as the calculation of the axion production rate is concerned, the static structure factor $S(\mathbf{Q})$ has already included the collective behavior of the solar medium. These two seemingly different descriptions reflect the same electromagnetic properties of the solar medium.

References [24–26] reproduced the same Primakoff production rate using thermal field theory while making the same Kramers-Kronig relations argument in the last step. It should be noted that in order for the Kramers-Kronig sum rules to work, the energy shift between the axion and the photon ω is assumed to be remarkably smaller than the solar temperature $T_\odot$, such that $1 - e^{-\omega/T_\odot} \simeq \omega/T_\odot$. Thus, a detailed numerical examination of this assumption is one of the inspirations for this work.

Recently, in Ref. [27] we applied the nonrelativistic linear response theory to the dynamic screening effect in the nondegenerate gas of the solar plasma associated with dark matter scattering. Under this framework, one no longer needs to add the dielectric function by hand since both the finite temperature effect and the many-body effect are inherently encapsulated in the dynamic structure factor $S(\mathbf{Q}, \omega)$. *Dynamic* means that a finite energy ω transfer (and thus a temporal variation) is taken into account in a scattering event, in contrast to the static case where the charged particles are regarded as fixed targets. This is important considering that the thermal velocities of electrons can reach $\sim 0.1c$ in the core of the Sun, which may bring a non-negligible Doppler energy shift in the Primakoff process. And more importantly, the screening and the collective effect (plasmon) are naturally incorporated into this dynamic structure factor $S(\mathbf{Q}, \omega)$. This method could be an alternative to the electromagnetic fluctuation description [23] and the thermal field theory approach [24–26] mentioned above.

Therefore, the purpose of this work is to apply the linear response theory approach [27] to the photon-axion conversion process on the Sun in order to investigate the implication of the recoil effect and the collective effect, and especially to numerically explore in detail to what extent the Kramers-Kronig sum rule argument is reliable to validate the calculation of the Primakoff conversion rate based on the static structure factor.

Discussion will proceed in the natural units, where $\hbar = c = k_B = 1$.

II. PRIMAKOFF EVENT RATE

We first introduce how we describe the Primakoff process in the context of the linear response theory that naturally encodes the relevant finite temperature physics and the many-body in-medium effect.

At the effective field theory (EFT) level, the interaction relevant for the Primakoff process is given as

$$\mathcal{L}_{a\gamma} = -\frac{g_{a\gamma}}{4} a F_{\mu\nu} \tilde{F}^{\mu\nu}, \tag{2}$$

where a is the axion field, $g_{a\gamma}$ represents the axion-photon coupling, and $F_{\mu\nu}$ and $\tilde{F}_{\mu\nu} = \frac{1}{2}\epsilon_{\mu\nu\rho\sigma}F^{\rho\sigma}$ are the electromagnetic field strength and its dual, respectively. Since the electrons and ions move nonrelativistically in the Sun, we express the relevant interactions in the nonrelativistic EFT. For instance, the electromagnetic field–electron interaction is written as

$$\mathcal{L}_{Ae} = -eA_0\psi_e^*\psi_e - \frac{ie}{2m_e}\mathbf{A}\cdot(\psi_e^*\overrightarrow{\nabla}\psi_e - \psi_e^*\overleftarrow{\nabla}\psi_e) - \frac{e^2}{2m_e}|\mathbf{A}|^2\cdot\psi_e^*\psi_e + \cdots, \tag{3}$$

where ψ_e is the nonrelativistic electron wave function. Considering that the second term on the right-hand side is subject to an electron velocity suppression $\frac{\nabla}{m_e} \sim v_e \sim \mathcal{O}(10^{-2}\text{–}10^{-1})$ in the solar medium (with m_e being the electron mass), and the longitudinal and transverse photon propagators do not mix under the random phase approximation (RPA), only the longitudinal component in the nonrelativistic effective electron-photon interaction A_0 (or, more specifically, the Coulomb interaction) is retained for the description of electron-electron (and electron-ion) interaction in this work. Thus, we only consider the components $-g_{a\gamma}a\epsilon^{ijk0}\partial_i A_j \partial_k A_0$ of the Lagrangian in Eq. (2) in the estimate of the Primakoff process in the Sun. While the A_0 component is responsible for the Coulomb interaction, $\{A_j\}$ are relevant for the transverse photon external legs.

The calculation of the Primakoff process shown in Fig. 1 depends on an accurate description of the electronic and ionic in-medium effect on the Sun. In this work, we invoke the linear response approach proposed in Ref. [27] to describe the screening effect on the Sun. Within this framework, the axion production rate for an incident photon with energy E_γ and momentum $\mathbf{p}_\gamma$ can be summarized by the following expression (see the Appendix for further details):

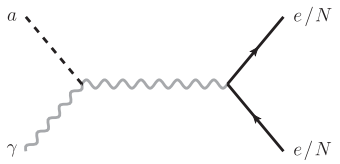

FIG. 1. Diagram for the Primakoff scattering process where a photon is converted into an axion in the Coulomb potential of charged particles (electron and ions). See the text for details.

$$\Gamma(\mathbf{p}_\gamma) = \int \mathrm{d}\omega \int \frac{\mathrm{d}^3 Q}{(2\pi)^3} \frac{g_{a\gamma}^2 |\mathbf{p}_\gamma \times \mathbf{Q}|^2}{8E_\gamma \sqrt{|\mathbf{p}_\gamma - \mathbf{Q}|^2 + m_a^2}} \frac{1}{Q^2} \delta\left(\sqrt{|\mathbf{p}_\gamma - \mathbf{Q}|^2 + m_a^2} - E_\gamma + \omega\right) \times \frac{(-2)}{1 - e^{-\omega/T_\odot}} \left[\frac{V_e \mathrm{Im}(\Pi_e)}{|1 - V_e\Pi_e - V_e \sum_i Z_i^2 \Pi_{N_i}|^2} + \frac{V_e \sum_i Z_i^2 \mathrm{Im}(\Pi_{N_i})}{|1 - V_e\Pi_e - V_e \sum_i Z_i^2 \Pi_{N_i}|^2}\right], \tag{4}$$

where $\alpha = e^2/4\pi$ is the electromagnetic fine structure constant, ω and $Q = |\mathbf{Q}|$ denote the energy and the magnitude of the momentum transfer to the solar medium, respectively, $V_e(Q) = 4\pi\alpha/Q^2$ is the electron Coulomb interaction in momentum space, and E_a (m_a) is the energy (mass) of the axion. The delta function represents the energy conservation in the scattering.

In this work, we only consider the case where the axion masses are so small (typically $\ll$ keV) compared to their energies that they can be effectively considered massless. Besides, Eq. (4) does not take into account the fact that photons inside a plasma have a nontrivial dispersion relation $E_\gamma^2 \simeq \omega_p^2 + |\mathbf{p}_\gamma|^2$, which means that photons propagating in the solar medium have an effective mass $\omega_p = \sqrt{4\pi\alpha n_e/m_e}$. Consequently, the conversion process is possible only for $E_\gamma > \omega_p$, and the plasmon mass effect becomes remarkable for energies $E_\gamma \gtrsim \omega_p$. However, since $\omega_p \approx 0.3$ keV is much smaller than the typical plasmon energy $3T_\odot \approx 4$ keV in the solar core [28], where the majority of axions are produced, the photons are also treated as massless in Eq. (4), which is in line with the treatment in Ref. [8]. Reference [29] provided an analytical conversion rate that adds the plasma frequency to the original expression in Ref. [8], based on which we verify that the plasmon mass effect brings a correction on the order of 10^{-4} between 1 and 12 keV.

The first and second terms in the square brackets correspond to the finite temperature many-body effect from the electrons and ions, respectively; while $\mathrm{Im}(\Pi_e)$ ($\mathrm{Im}(\Pi_{N_i})$) is responsible for the thermal movement of the electrons (ions), the denominator describes the screening [27]. Π_e denotes the electron one-particle-irreducible diagram in the RPA, which is approximated as the bubble diagram. For the nondegenerate electron gas in the Sun, Π_e can be expressed as [27]

$$\Pi_e(Q,\omega) = -\frac{n_e}{Q}\sqrt{\frac{m_e}{2T_\odot}}\left\{\Phi\left[\sqrt{\frac{m_e}{2T_\odot}}\left(\frac{\omega}{Q} + \frac{Q}{2m_e}\right)\right] - \Phi\left[\sqrt{\frac{m_e}{2T_\odot}}\left(\frac{\omega}{Q} - \frac{Q}{2m_e}\right)\right]\right\} - i n_e \sqrt{\frac{2\pi}{m_e T_\odot}}\left(\frac{m_e}{Q}\right) \exp\left[-\left(\frac{m_e^2\omega^2}{Q^2} + \frac{Q^2}{4}\right)\frac{1}{2m_e T_\odot}\right] \sinh\left[\frac{\omega}{2T_\odot}\right], \tag{5}$$

where n_e is the number density of the electron gas and the function Φ is defined as the Cauchy principal value of the integration [30],

$$\Phi(x) \equiv \mathcal{P}\int_{-\infty}^{+\infty} \frac{\mathrm{d}y}{\sqrt{\pi}} \frac{e^{-y^2}}{x - y}. \tag{6}$$

Similarly, Π_{N_i} denotes the bubble diagram of the ith ion species carrying the charge $Z_i e$. At the RPA level, Π_{N_i} can be obtained by simply replacing n_e and m_e with ion number density n_{N_i} and ion mass m_{N_i} in Eq. (5). Contributions from all solar ion species are included in Eq. (4). In order to describe the collective behavior of the solar medium, we introduce a nondimensional function $\mathcal{F}(Q,\omega)$, which represents the second line in Eq. (4). Interestingly, in Fig. 2 a strong resonance structure is observed in the parameter area where the real part approaches zero in the denominator in Eq. (4), which corresponds to the absorption of a longitudinal plasmon in the process $\gamma_t + \gamma_l \to a$. At the symmetric position in the upper half plane there is another pole corresponding to the emission of a plasmon in the process $\gamma_t \to \gamma_l + a$. As long as kinematically allowed, such collective behavior may significantly alter the fixed-electron picture of the axion production process. $\mathcal{F}(Q,\omega)$ provides a complete description of the longitudinal plasmon behavior far beyond the approximated dispersion relation $\omega^2 \backsimeq \omega_p^2 + 3(T_\odot/m_e)Q^2$ [8].

Based on the axion production rate of Eq. (4), the differential axion flux reaching Earth can then be written as the convolution of the differential transition rate with the photon blackbody distribution in the Sun,

$$\frac{\mathrm{d}\Phi_a(E_a)}{\mathrm{d}E_a} = \frac{1}{4\pi d_\odot^2}\int_0^{R_\odot} \mathrm{d}^3 r \int \frac{\mathrm{d}E_\gamma}{\pi^2} \frac{E_\gamma^2}{e^{E_\gamma/T_\odot} - 1} \frac{\mathrm{d}\Gamma(\mathbf{p}_\gamma)}{\mathrm{d}E_a}, \tag{7}$$

with the Sun-Earth distance $d_\odot$ and the solar radius $R_\odot$.

In the static screening prescription, since the energy of the incident photon equals that of the axion, the differential axion flux is given as [10]

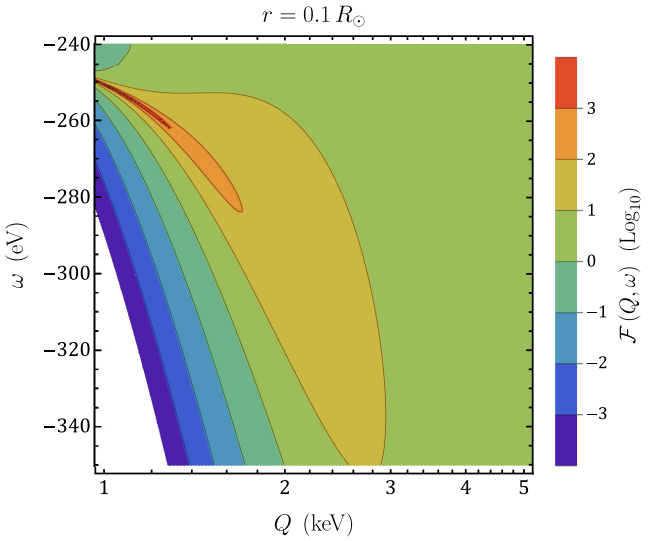

FIG. 2. The factor $\mathcal{F}(Q,\omega)$ that demonstrates the longitudinal plasmon resonance of the solar medium at radius $r = 0.1R_\odot$ (with $R_\odot$ being the solar radius). The highly resonant "line" (below $Q < 1$ keV) is too narrow to be shown in the plot. It is evident that such plasmons suffer strong damping for $Q \gtrsim 2$ keV. See the text for details.

$$\frac{d\Phi_a(E_a)}{dE_a} = \frac{1}{4\pi d_\odot^2}\int_0^{R_\odot} d^3r \frac{1}{\pi^2}\frac{E_a^2}{e^{E_a/T_\odot}-1}\Gamma_s, \qquad (8)$$

with the relevant static photon-axion conversion rate

$$\Gamma_s = \frac{T_\odot \kappa^2 g_{a\gamma}^2}{32\pi}\left[\left(1+\frac{\kappa^2}{4E_a^2}\right)\ln\left(1+\frac{4E_a^2}{\kappa^2}\right)-1\right], \qquad (9)$$

where $\kappa^2 = (4\pi\alpha/T_\odot)(n_e + \sum_i Z_i^2 n_{N_i})$ is the square of the Debye-Hückel scale.

III. AXION FLUX ON EARTH

Equipped with the above formulation that describes the solar in-medium effect with the linear response theory, now we are in the position to calculate the axion flux at terrestrial detectors.

In the left panel of Fig. 3, we compare the solar Primakoff axion fluxes on Earth computed with the linear response theory in Eq. (7) and with the static screening description of the Coulomb interaction in Eq. (8).

These spectra are obtained by integrating the contributions from the charged particles in every thin shell in the Sun, based on the standard Sun model AGSS09 [31]. In practice, the solar radius is discretized into 100 slices, and the 29 most common solar elements are included in our computation. In addition, we assume that these solar elements are fully ionized.

While in the left panel of Fig. 3 it is observed that the average (4.2 keV) and the maximum (3.0 keV) of the Primakoff axion energy distribution remain unchanged, the differential rate is only 1% to 2% lower than the calculation based on the static structure factor in the energy range of 2 to 12 keV. It is quite a surprising result, given that the denominator term $|1 - V_e\Pi_e - V_e\sum_i Z_i^2\Pi_{N_i}|^{-2}$ in Eq. (4)

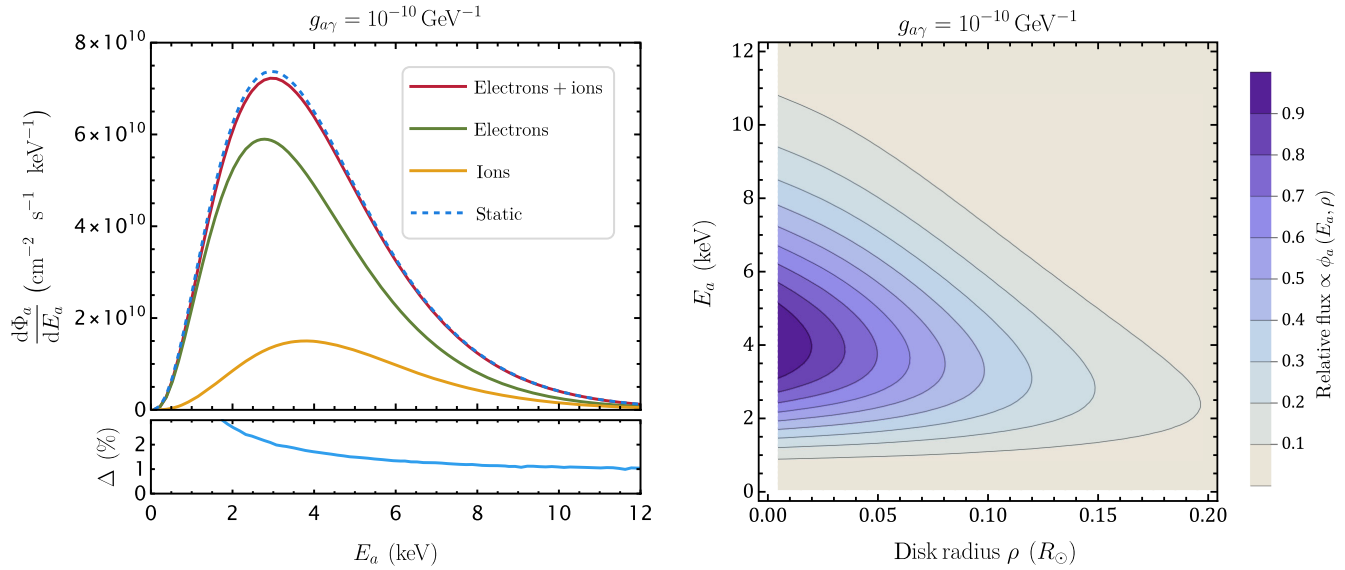

FIG. 3. Left panel: solar Primakoff axion spectra on Earth calculated with the static structure factor (dashed blue line), and with the dynamic structure factor (red line) that consists of the contributions from electrons (green line) and ions (orange line), for a benchmark coupling strength $g_{a\gamma} = 10^{-10}$ GeV^{-1}. Δ (in %) represents the relative difference between the two approaches, i.e., $\Delta \equiv (\text{static} - \text{dynamic})/\text{static}$. Right panel: contour plot of the solar axion surface luminosity, normalized to its maximum value, depending on the radius ρ on the solar disk and energy E_a. See the text for details.

asymptotes to the Debye screening form $(1+\kappa^2/Q^2)^{-2}$ in the limit $\omega \to 0$, where it brings a stronger screening than the static structure factor $(1+\kappa^2/Q^2)^{-1}$ in Eq. (1); the contributions of the recoil effect and the collective effect must coincidentally make up this loss to keep the total rate unchanged.

Such a coincidence would be difficult if there were no intrinsic relation protecting the total rate, especially considering that, in contrast to the static screening picture, where the contributions from the electrons and ions are in scale to the electric charge densities n_e and $\sum_i Z_i^2 n_{N_i}$ and hence a larger part of the conversion comes from the scattering with ions, it turns out that the collective electrons contribute dominantly to the total Primakoff axion flux in the dynamic screening picture. Thus, our results actually confirm the validity of the Kramers-Kronig sum rule argument in Ref. [23] up to a percent-level correction.

In the right panel of Fig. 3, we also present the differential solar axion flux (using the dynamic structure factor) as an apparent surface luminosity $\phi_a(E_a,\rho)$ of the solar disk [29,32,33],

$$\phi_a(E_a,\rho) = \frac{R_\odot^3}{2\pi^3 d_\odot^2}\int_\rho^1 \frac{\tilde{r}\mathrm{d}\tilde{r}}{\sqrt{\tilde{r}^2-\rho^2}} \times \int \frac{\mathrm{d}E_\gamma}{\pi^2}\frac{E_\gamma^2}{e^{E_\gamma/T_\odot}-1}\frac{\mathrm{d}\Gamma(\mathbf{p}_\gamma)}{\mathrm{d}E_a}, \tag{10}$$

where the dimensionless quantities $\tilde{r} = r/R_\odot$ and ρ represent the radial position of the conversion process and the distance from the center of the solar disk, respectively.

IV. DISCUSSIONS AND CONCLUSIONS

In order to further explore the many-body effect in the solar medium in detail, in Fig. 4 we present the differential axion production rates for photon energies $E_\gamma = 2$ and 8 keV at the solar radius $r = 0.1R_\odot$, respectively, with the benchmark coupling $g_{a\gamma} = 10^{-10}$ GeV^{-1}. While the spectra of heavy ions are found to narrowly center at the photon energies, behaving like static targets, it is intriguingly observed that the non-negligible electron movement in the inner part of the Sun can bring an energy shift up to $\mathcal{O}(0.1)$ keV from the initial photon energies. For one thing, the two peaks in Fig. 4 correspond to the absorption and emission of a longitudinal plasmon at $\omega \simeq \pm\sqrt{4\pi\alpha n_e/m_e}$ in the Sun, respectively. That is, a considerable part of the Primakoff processes proceed in conjunction with absorbance and emission of a plasmon. For another, a broadening width of around 0.4 keV is also clearly seen due to the thermal movement of the electrons. While such a finite spread of the photon energy may not bring a noticeable change to the total spectrum of the solar axion, the strength of the resonance, i.e., the implication of the collective effect, can be determined only with a concrete calculation.

To conclude, in this paper we have applied the linear response theory formalism for a delicate estimate of the Primakoff photon-axion conversion rate in the Sun. Based on this method, progress is gained in two aspects: (1) we provide an up-to-date panoramic description of the dynamic Primakoff process, which is explicitly shown to be a combination of the decay process $\gamma_t \to \gamma_l + a$, the plasma coalescence process $\gamma_t + \gamma_l \to a$, and the individual Primakoff process $\gamma_t + e/N \to a + e/N$, and (2) beyond

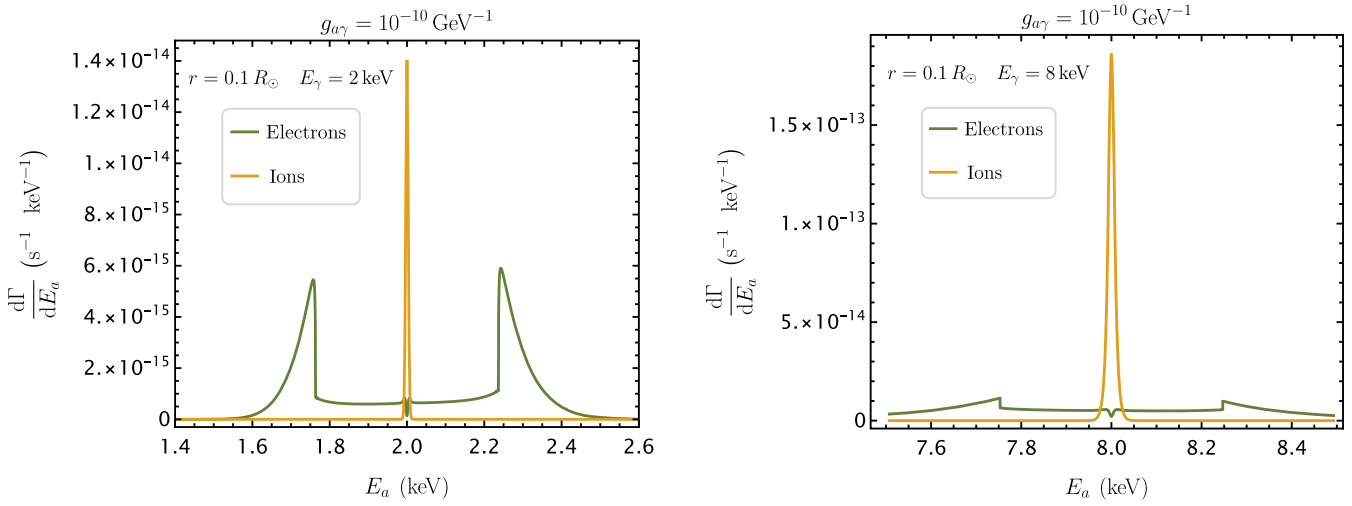

FIG. 4. Primakoff differential photon-axion conversion rates for photon energies $E_\gamma = 2$ keV (left panel) and 8 keV (right panel) at the solar radius $r = 0.1R_\odot$, with contributions from electrons (green lines) and ions (orange lines), respectively. The plasmon absorption and emission peaks are clearly seen.

the approximate Kramers-Kronig sum rules, we numerically calculate the relevant terrestrial axion flux due to the Primakoff process, and the flux is found to be around 1% to 2% lower than the previous estimation based on the static structure factor.

Lastly, this dynamic response-oriented approach can be further applied to other axion production mechanisms such as electron- and ion-bremsstrahlung processes in the Sun, where a systematic treatment of the screening and collective effects is also highly useful.

APPENDIX: FORMULATION FOR THE PRIMAKOFF SCATTERING EVENT RATE ON THE SUN

In this appendix we give a detailed derivation of the formulas in the main text that describe the Primakoff photon-axion conversion process in the Sun. In the nonrelativistic regime, it is convenient to discuss this process in the *Coulomb gauge*.

We start with the $\mathcal{T}$ matrix for the Primakoff process where a photon (with momentum $\mathbf{p}_\gamma$ and polarization λ) scatters with a nonrelativistically moving electron (illustrated in Fig. 1), emitting an axion with momentum $\mathbf{p}_a$, i.e.,

$$\langle \mathbf{p}_a, i|i\mathcal{T}|\mathbf{p}_\gamma,\lambda;j\rangle = ig_{a\gamma}e\frac{(\mathbf{p}_\gamma\times\mathbf{p}_a)\cdot\hat{\boldsymbol{\varepsilon}}^\lambda(\mathbf{p}_\gamma)}{|\mathbf{p}_\gamma-\mathbf{p}_a|^2} \times\langle i|e^{i(\mathbf{p}_\gamma-\mathbf{p}_a)\cdot\hat{\mathbf{x}}}|j\rangle 2\pi\delta(E_\gamma-E_a-\varepsilon_i+\varepsilon_j), \tag{A1}$$

where $\hat{\boldsymbol{\varepsilon}}^\lambda(\mathbf{p}_\gamma)$ is the polarization vector for the incident photon, which satisfies the complete and orthonormal relation, i.e., $\sum_{\lambda=\pm1}\hat{\boldsymbol{\varepsilon}}^{\lambda i}(\mathbf{p}_\gamma)\hat{\boldsymbol{\varepsilon}}^{\lambda j*}(\mathbf{p}_\gamma)=\delta^{ij}-p_\gamma^i p_\gamma^j/|\mathbf{p}_\gamma|^2$, and $\mathbf{p}_\gamma\cdot\hat{\boldsymbol{\varepsilon}}^{\pm1}(\mathbf{p}_\gamma)=0$; E_γ, E_a, ε_i, and ε_j represent the energies of the photon, the emitted axion, the initial and the final state of the electron, respectively.

Then we take into account the many-body effect of the solar medium with the approach adopted in Refs. [27,34]. To this end, we resort to the linear response theory, whereby the Primakoff event rate for a photon with momentum $\mathbf{p}_\gamma$ (by averaging over the initial states and summing over the final states) is written as follows (for simplicity, here we assume that only one type of ions with charge Ze and mass m_N are present):

$$\begin{aligned}
\Gamma(\mathbf{p}_\gamma) &= \sum_{i,j}\int \mathrm{d}\omega\,\delta(\omega-\varepsilon_i+\varepsilon_j)\int \mathrm{d}^3Q\,\delta^{(3)}(\mathbf{Q}+\mathbf{p}_a-\mathbf{p}_\gamma)\int\frac{\mathrm{d}^3p_a}{2E_a(2\pi)^3}\left(\frac{g_{a\gamma}e}{Q^2}\right)^2\frac{1}{2}\sum_{\lambda=\pm1}\frac{|(\mathbf{p}_\gamma\times\mathbf{p}_a)\cdot\hat{\boldsymbol{\varepsilon}}^\lambda(\mathbf{p}_\gamma)|^2}{2E_\gamma}\\
&\times\frac{1}{V}\int_V \mathrm{d}^3x\,\mathrm{d}^3x' p_j\langle j|e^{-i\mathbf{Q}\cdot\mathbf{x}}[\hat{\rho}_e+(-Z)\hat{\rho}_N](\mathbf{x})|i\rangle\langle i|e^{i\mathbf{Q}\cdot\mathbf{x}'}[\hat{\rho}_e+(-Z)\hat{\rho}_N](\mathbf{x}')|j 2\pi\delta(E_\gamma-E_a-\omega)\\
&= \int\mathrm{d}\omega\int\frac{\mathrm{d}^3Q}{(2\pi)^3}\frac{4\pi\alpha}{Q^4}\frac{g_{a\gamma}^2|\mathbf{p}_\gamma\times\mathbf{Q}|^2}{8E_\gamma\sqrt{|\mathbf{p}_\gamma-\mathbf{Q}|^2+m_a^2}}\frac{1}{V}\int_V\mathrm{d}^3x\,\mathrm{d}^3x' e^{-i\mathbf{Q}\cdot(\mathbf{x}-\mathbf{x}')}\int_{-\infty}^{+\infty}e^{i\omega(0-t)}\mathrm{d}t[\langle\hat{\rho}_{eI}(\mathbf{x},0)\hat{\rho}_{eI}(\mathbf{x}',t)\rangle\\
&+(-Z)\langle\hat{\rho}_{eI}(\mathbf{x},0)\hat{\rho}_{NI}(\mathbf{x}',t)+(-Z)\langle\hat{\rho}_{NI}(\mathbf{x},0)\hat{\rho}_{eI}(\mathbf{x}',t)+(-Z)^2\langle\hat{\rho}_{NI}(\mathbf{x},0)\hat{\rho}_{NI}(\mathbf{x}',t)]\delta(E_\gamma-E_a-\omega)\\
&= \int\mathrm{d}\omega\int\frac{\mathrm{d}^3Q}{(2\pi)^3}\frac{4\pi\alpha}{Q^4}\frac{g_{a\gamma}^2|\mathbf{p}_\gamma\times\mathbf{Q}|^2}{8E_\gamma\sqrt{|\mathbf{p}_\gamma-\mathbf{Q}|^2+m_a^2}}\frac{(-2)}{1-e^{-\omega/T_\odot}}\mathrm{Im}[\chi^{\mathrm{r}}_{\hat{\rho}_e\hat{\rho}_e}+(-Z)\chi^{\mathrm{r}}_{\hat{\rho}_e\hat{\rho}_N}+(-Z)\chi^{\mathrm{r}}_{\hat{\rho}_N\hat{\rho}_e}+(-Z)^2\chi^{\mathrm{r}}_{\hat{\rho}_N\hat{\rho}_N}]\\
&\times\delta\left(\sqrt{|\mathbf{p}_\gamma-\mathbf{Q}|^2+m_a^2}-E_\gamma+\omega\right)\\
&= \int\mathrm{d}\omega\int\frac{\mathrm{d}^3Q}{(2\pi)^2}\frac{4\pi\alpha}{Q^4}\frac{g_{a\gamma}^2|\mathbf{p}_\gamma\times\mathbf{Q}|^2}{8E_\gamma\sqrt{|\mathbf{p}_\gamma-\mathbf{Q}|^2+m_a^2}}\frac{(-2)}{1-e^{-\omega/T_\odot}}\left[\frac{\mathrm{Im}(\Pi_e)}{|1-V_e\Pi_e-V_eZ^2\Pi_N|^2}+\frac{Z^2\mathrm{Im}(\Pi_N)}{|1-V_e\Pi_e-V_eZ^2\Pi_N|^2}\right]\\
&\times\delta\left(\sqrt{|\mathbf{p}_\gamma-\mathbf{Q}|^2+m_a^2}-E_\gamma+\omega\right),
\end{aligned}\tag{A2}$$

where we introduce the density operators for electrons $\hat{\rho}_e(\mathbf{x})\equiv\hat{\psi}_e^\dagger(\mathbf{x})\hat{\psi}_e(\mathbf{x})$ and ions $\hat{\rho}_N(\mathbf{x})\equiv\hat{\psi}_N^\dagger(\mathbf{x})\hat{\psi}_N(\mathbf{x})$, p_j represents the thermal distribution of the initial state $|j\rangle$, the symbol $\langle\cdots\rangle$ represents the thermal average, $\hat{\rho}_{eI}(\mathbf{x}',t)\equiv e^{i\hat{H}_0t}\hat{\rho}_e(\mathbf{x}')e^{-i\hat{H}_0t}$ ($\hat{\rho}_{NI}(\mathbf{x},t)\equiv e^{i\hat{H}_0t}\hat{\rho}_N(\mathbf{x})e^{-i\hat{H}_0t}$), with $\hat{H}_0$ being the unperturbed Hamiltonian of the medium system, and V is the volume of the solar medium under consideration, which is only an intermediate quantity and is canceled in the final expression of the event rate.

In addition, in the above derivation we invoke the fluctuation-dissipation theorem

$$
\begin{aligned}
S_{\hat{\rho}\hat{\rho}}(\mathbf{Q},\omega) &= \frac{1}{V}\int_V \mathrm{d}^3x\,\mathrm{d}^3x' e^{-i\mathbf{Q}\cdot(\mathbf{x}-\mathbf{x}')}\int_{-\infty}^{+\infty}\mathrm{d}t\, e^{i\omega(0-t)} \\
&\quad\times\langle\hat{\rho}_I(\mathbf{x},0)\hat{\rho}_I(\mathbf{x}',t)\rangle \\
&= i\frac{[\chi_{\hat{\rho}\hat{\rho}}(\mathbf{Q},\omega+i0^+)-\chi_{\hat{\rho}\hat{\rho}}(\mathbf{Q},\omega-i0^+)]}{1-e^{-\omega/T}} \\
&= \frac{-2\mathrm{Im}[\chi^{\mathrm{r}}_{\hat{\rho}\hat{\rho}}(\mathbf{Q},\omega)]}{1-e^{-\omega/T}},
\end{aligned}
\tag{A3}
$$

where T represents temperature and $\hat{\rho}$ generally stands for $\hat{\rho}_e$ and $\hat{\rho}_N$, so $S_{\hat{\rho}\hat{\rho}}(\mathbf{Q},\omega)$ represents the dynamic structure factor associated with the density-density correlation. In practice [35], one first evaluates the master function $\chi_{\hat{\rho}\hat{\rho}}(\mathbf{Q},z)$ using the Matsubara Green's function within the framework of finite temperature field theory, then obtains the retarded polarizability function $\chi^{\mathrm{r}}_{\hat{\rho}\hat{\rho}}(\mathbf{Q},\omega)$ by performing the analytic continuation $\chi^{\mathrm{r}}_{\hat{\rho}\hat{\rho}}(\mathbf{Q},\omega)=\chi_{\hat{\rho}\hat{\rho}}(\mathbf{Q},z\to\omega+i0^+)$.

Here we take the retarded correlation function $\chi^{\mathrm{r}}_{\hat{\rho}_e\hat{\rho}_N}$ as an example to illustrate how the calculation is carried out, with the calculation presented as the sum of all possible diagrams that connect the two density operators as follows:

$\chi^{\mathrm{r}}_{\hat{\rho}_e\hat{\rho}_N} =$ 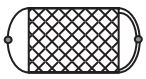

$=$ 

$=$ 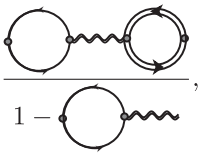

(A4)

where  and  represent the electron and ion pair-bubble diagrams, respectively, i.e., Π_e and Π_N at the RPA level [see Eq. (5)], and the double wavy line

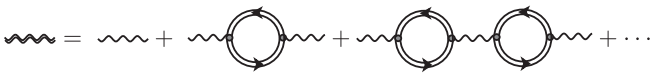

$$
\begin{aligned}
&= V_e + V_e(-Z)\,\Pi_N V_e(-Z) \\
&\quad + V_e(-Z)\,\Pi_N V_e(-Z)^2\,\Pi_N V_e(-Z)+\cdots \\
&= \frac{V_e}{1-Z^2\,V_e\,\Pi_N}
\end{aligned}
\tag{A5}
$$

represents the electron Coulomb interaction screened by the ions [the single wavy line corresponds to the Coulomb interaction $V_e(Q)$]. Then Eq. (A4) can be explicitly written as

$$
\chi^{\mathrm{r}}_{\hat{\rho}_e\hat{\rho}_N} = \frac{\Pi_e(-Z)V_e\Pi_N}{1-V_e\Pi_e-Z^2V_e\Pi_N}. \tag{A6}
$$

The above discussion can be extended to obtain the retarded correlation functions $\chi^{\mathrm{r}}_{\hat{\rho}_N\hat{\rho}_e}$ and $\chi^{\mathrm{r}}_{\hat{\rho}_N\hat{\rho}_N}$ such that

$$
\chi^{\mathrm{r}}_{\hat{\rho}_N\hat{\rho}_e} = \chi^{\mathrm{r}}_{\hat{\rho}_e\hat{\rho}_N} \tag{A7}
$$

and

$$
\chi^{\mathrm{r}}_{\hat{\rho}_N\hat{\rho}_N} = \frac{(1-V_e\Pi_e)\Pi_N}{1-V_e\Pi_e-V_eZ^2\Pi_N}. \tag{A8}
$$

In addition, in Ref. [27], we already derived

$$
\chi^{\mathrm{r}}_{\hat{\rho}_e\hat{\rho}_e} = \frac{\Pi_e(1-Z^2V_e\Pi_N)}{1-V_e\Pi_e-Z^2V_e\Pi_N}. \tag{A9}
$$

Thus, by combining all these terms it is straightforward to verify that

$$
\begin{aligned}
&\chi^{\mathrm{r}}_{\hat{\rho}_e\hat{\rho}_e}+(-Z)\chi^{\mathrm{r}}_{\hat{\rho}_e\hat{\rho}_N}+(-Z)\chi^{\mathrm{r}}_{\hat{\rho}_N\hat{\rho}_e}+(-Z)^2\chi^{\mathrm{r}}_{\hat{\rho}_N\hat{\rho}_N} \\
&\quad=\frac{\Pi_e}{1-V_e\Pi_e-Z^2V_e\Pi_N}+\frac{Z^2\Pi_N}{1-V_e\Pi_e-Z^2V_e\Pi_N}
\end{aligned}
\tag{A10}
$$

in Eq. (A2). As noted in Ref. [27], this expression encodes both the thermal movement and the in-medium effect of the electrons and ions.

In the practical computation of Eq. (A2), we first integrate out the polar angle of $\mathbf{Q}$ with respect to the direction of the photon momentum $\mathbf{p}_\gamma$, which is fixed as the z axis in the spherical coordinate system. We then take a variable transformation from $\cos\theta_{\mathbf{Qp}_\gamma}$ to the variable $E_a=\sqrt{|\mathbf{p}_\gamma-\mathbf{Q}|^2+m_a^2}$, along with the corresponding Jacobian

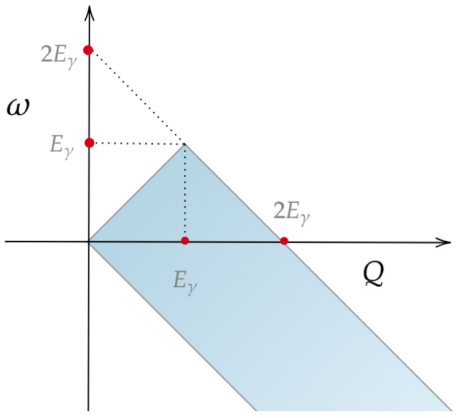

FIG. 5. The effective integral area relevant for the Primakoff event rate of Eq. (A12). See the text for details.

$$\left|\frac{\mathrm{d}\cos\theta_{\mathbf{Q}\mathbf{p}_\gamma}}{\mathrm{d}E_a}\right| = \frac{p_\gamma Q}{E_a}. \tag{A11}$$

With this change of variable, the term proportional to $\sin^2\theta_{\mathbf{Q}\mathbf{p}_\gamma}$ in Eq. (A2), i.e., $|\mathbf{p}_\gamma \times \mathbf{Q}|^2$, can be rewritten as $p_\gamma^2 Q^2 - [(E_a^2 - m_a^2 - p_\gamma^2 - Q^2)^2/4]$. Thus, Eq. (A2) is further expressed as

$$\begin{aligned}
\Gamma(\mathbf{p}_\gamma) &= \int \mathrm{d}\omega \int \frac{\mathrm{d}^3 Q}{(2\pi)^3} \frac{4\pi\alpha}{Q^4} \frac{g_{a\gamma}^2 |\mathbf{p}_\gamma \times \mathbf{Q}|^2}{8E_\gamma \sqrt{|\mathbf{p}_\gamma - \mathbf{Q}|^2 + m_a^2}} \frac{(-2)}{1 - e^{-\omega/T_\odot}} \left[\frac{\mathrm{Im}(\Pi_e)}{|1 - V_e\Pi_e - V_e Z^2 \Pi_N|^2} + \frac{Z^2 \mathrm{Im}(\Pi_N)}{|1 - V_e\Pi_e - V_e Z^2\Pi_N|^2}\right] \\
&\quad \times \delta(\sqrt{|\mathbf{p}_\gamma - \mathbf{Q}|^2 + m_a^2} - E_\gamma + \omega) \\
&= \int \mathrm{d}\omega \int \frac{Q\mathrm{d}Q}{(2\pi)^2} \frac{4\pi\alpha}{Q^4} \frac{g_{a\gamma}^2}{8E_\gamma^2} \frac{(-2)}{1 - e^{-\omega/T_\odot}} \left[\frac{\mathrm{Im}(\Pi_e)}{|1 - V_e\Pi_e - V_e Z^2 \Pi_N|^2} + \frac{Z^2 \mathrm{Im}(\Pi_N)}{|1 - V_e\Pi_e - V_e Z^2\Pi_N|^2}\right] \\
&\quad \times \int_{E_-}^{E^+} \mathrm{d}E_a \left[p_\gamma^2 Q^2 - \frac{(E_a^2 - m_a^2 - p_\gamma^2 - Q^2)^2}{4}\right] \delta(E_a - E_\gamma + \omega) \\
&= \int \mathrm{d}\omega \int \frac{Q\mathrm{d}Q}{(2\pi)^2} \frac{4\pi\alpha}{Q^4} \frac{g_{a\gamma}^2}{8E_\gamma^2} \frac{(-2)}{1 - e^{-\omega/T_\odot}} \left[\frac{\mathrm{Im}(\Pi_e)}{|1 - V_e\Pi_e - V_e Z^2 \Pi_N|^2} + \frac{Z^2 \mathrm{Im}(\Pi_N)}{|1 - V_e\Pi_e - V_e Z^2\Pi_N|^2}\right] \\
&\quad \times \left[p_\gamma^2 Q^2 - \frac{(\omega^2 - 2\omega p_\gamma - Q^2)^2}{4}\right] \Theta(Q + \omega) \cdot [\Theta(Q - \omega)\Theta(p_\gamma - Q) + \Theta(2E_\gamma - Q - \omega)\Theta(Q - p_\gamma)],
\end{aligned} \tag{A12}$$

where $E_\pm = \sqrt{(p_\gamma \pm Q)^2 + m_a^2}$. On the last line, we take $m_a \to 0$, and Θ is the Heaviside step function. The integral area on the $Q - \omega$ plane corresponding to these step functions is shown in Fig. 5 for illustration. In the last step, we generalize the above expression to the multiple atom species in the Sun [as the sum over isotopes in the square brackets in Eq. (4)].

[1] R. D. Peccei and H. R. Quinn, *CP* conservation in the presence of instantons, Phys. Rev. Lett. **38**, 1440 (1977).
[2] S. Weinberg, A new light boson?, Phys. Rev. Lett. **40**, 223 (1978).
[3] F. Wilczek, Problem of strong *P* and *T* invariance in the presence of instantons, Phys. Rev. Lett. **40**, 279 (1978).
[4] J. Preskill, M. B. Wise, and F. Wilczek, Cosmology of the invisible axion, Phys. Lett. **120B**, 127 (1983).
[5] L. F. Abbott and P. Sikivie, A cosmological bound on the invisible axion, Phys. Lett. **120B**, 133 (1983).
[6] M. Dine and W. Fischler, The not-so-harmless axion, Phys. Lett. **120B**, 137 (1983).
[7] D. Cadamuro and J. Redondo, Cosmological bounds on pseudo Nambu-Goldstone bosons, J. Cosmol. Astropart. Phys. 02 (2012) 032.
[8] G. G. Raffelt, Astrophysical axion bounds diminished by screening effects, Phys. Rev. D **33**, 897 (1986).
[9] G. G. Raffelt, Astrophysical methods to constrain axions and other novel particle phenomena, Phys. Rep. **198**, 1 (1990).
[10] G. G. Raffelt, *Stars as Laboratories for Fundamental Physics: The Astrophysics of Neutrinos, Axions, and Other Weakly Interacting Particles* (University of Chicago Press, Chicago, 1996).
[11] L. D. Duffy and K. van Bibber, Axions as dark matter particles, New J. Phys. **11**, 105008 (2009).
[12] M. Kawasaki and K. Nakayama, Axions: Theory and cosmological role, Annu. Rev. Nucl. Part. Sci. **63**, 69 (2013).
[13] D. J. E. Marsh, Axion cosmology, Phys. Rep. **643**, 1 (2016).
[14] P. W. Graham, I. G. Irastorza, S. K. Lamoreaux, A. Lindner, and K. A. van Bibber, Experimental searches for the axion and axion-like particles, Annu. Rev. Nucl. Part. Sci. **65**, 485 (2015).
[15] H. Primakoff, Photoproduction of neutral mesons in nuclear electric fields and the mean life of the neutral meson, Phys. Rev. **81**, 899 (1951).
[16] D. A. Dicus, E. W. Kolb, V. L. Teplitz, and R. V. Wagoner, Astrophysical bounds on the masses of axions and Higgs particles, Phys. Rev. D **18**, 1829 (1978).
[17] S. Dimopoulos, J. A. Frieman, B. W. Lynn, and G. D. Starkman, Axiorecombination: A new mechanism for stellar axion production, Phys. Lett. B **179**, 223 (1986).
[18] J. Redondo, Solar axion flux from the axion-electron coupling, J. Cosmol. Astropart. Phys. 12 (2013) 008.
[19] M. Dine, W. Fischler, and M. Srednicki, A simple solution to the strong *CP* problem with a harmless axion, Phys. Lett. **104B**, 199 (1981).

[20] A. R. Zhitnitsky, On possible suppression of the axion hadron interactions, Sov. J. Nucl. Phys. **31**, 260 (1980).
[21] J. E. Kim, Weak interaction singlet and strong *CP* invariance, Phys. Rev. Lett. **43**, 103 (1979).
[22] M. A. Shifman, A. I. Vainshtein, and V. I. Zakharov, Can confinement ensure natural *CP* invariance of strong interactions?, Nucl. Phys. **B166**, 493 (1980).
[23] G. G. Raffelt, Plasmon decay into low mass bosons in stars, Phys. Rev. D **37**, 1356 (1988).
[24] T. Altherr, Plasmon effects in light scalar and pseudoscalar emission from a supernova, Ann. Phys. (N.Y.) **207**, 374 (1991).
[25] T. Altherr, E. Petitgirard, and T. de Rio Gaztelurrutia, Photon propagation in dense media, Astropart. Phys. **1**, 289 (1993).
[26] T. Altherr, E. Petitgirard, and T. del Rio Gaztelurrutia, Axion emission from red giants and white dwarfs, Astropart. Phys. **2**, 175 (1994).
[27] Z.-L. Liang and P. Zhang, The linear response theory approach to the sub-GeV dark matter in the Sun, J. Cosmol. Astropart. Phys. 12 (2023) 009.
[28] J. K. Vogel and I. G. Irastorza, *Solar Production of Ultralight Bosons* (Springer International Publishing, Cham, Switzerland, 2023).
[29] S. Hoof, J. Jaeckel, and L. J. Thormaehlen, Quantifying uncertainties in the solar axion flux and their impact on determining axion model parameters, J. Cosmol. Astropart. Phys. 09 (2021) 006.
[30] A. Fetter and J. Walecka, *Quantum Theory of Many-Particle Systems*, Dover Books on Physics (Dover Publications, New York, 2012).
[31] A. Serenelli, S. Basu, J. W. Ferguson, and M. Asplund, New solar composition: The problem with solar models revisited, Astrophys. J. **705**, L123 (2009).
[32] CAST Collaboration, An improved limit on the axion-photon coupling from the CAST experiment, J. Cosmol. Astropart. Phys. 04 (2007) 010.
[33] S. Hoof, J. Jaeckel, and L. J. Thormaehlen, Axion helioscopes as solar thermometers, J. Cosmol. Astropart. Phys. 10 (2023) 024.
[34] Z.-L. Liang, C. Mo, and P. Zhang, In-medium screening effects for the galactic halo and solar-reflected dark matter detection in semiconductor targets, Phys. Rev. D **104**, 096001 (2021).
[35] H. Bruus and K. Flensberg, *Many-Body Quantum Theory in Condensed Matter Physics: An Introduction*, Oxford Graduate Texts (Oxford University Press, Oxford, 2004).